Energy harvesting with dielectric elastomer tubes: active and (responsive materials-based) passive approaches

To cite this article: Tamara Hanuhov *et al* 2024 *Smart Mater. Struct.* **33** 055004

OPEN ACCESS
IOP Publishing
Smart Materials and Structures
Smart Mater. Struct. **33** (2024) 055004 (11pp)
https://doi.org/10.1088/1361-665X/ad37b7

Energy harvesting with dielectric elastomer tubes: active and (responsive materials-based) passive approaches

Tamara Hanuhov[1], **Roberto Brighenti**[2] **and Noy Cohen**[1,*]

[1] Department of Materials Science and Engineering, Technion—Israel Institute of Technology, Haifa 3200003, Israel
[2] Department of Civil and Environmental Engineering, University of Florence, Via di S. Marta 3, 50139 Florence, Italy

E-mail: noyco@technion.ac.il and roberto.brighenti@unifi.it

Received 24 December 2023, revised 22 February 2024
Accepted for publication 24 March 2024
Published 3 April 2024

Abstract

Mechanical to electrical energy conversion is a well-established energy transduction approach. However, cases in which a mechanical energy source is not available call for new approaches to harvest electrical energy. In the present study, we demonstrate energy harvesting in soft dielectric elastomer (DE) tubes. Broadly, energy harvesting is obtained through inflation of the tube, electrical charging of the DE layer, and deflation, which results in a decrease in capacitance and an increase in voltage. We propose two methods to mechanically charge (or inflate) the system: (1) active, in which the tube is inflated through the application of mechanical pressure, and (2) passive, in which a passive cylindrical component placed inside the DE tube deforms radially in response to an environmental stimulus such as thermal excitation or water uptake and inflates the DE tube. To demonstrate passive charging, we consider gels as the passive component and employ well-known models with the properties of the commonly employed DE VHB 4910 to simulate the mechanical response of the system and estimate the harvested electrical energy. Our findings reveal that energy-densities in the order of $\sim$10–50 mJ cm^{-3} can be harvested. The proposed approach and the inclusion of a passive component to mechanically charge the system opens new opportunities to generate energy in environments lacking traditional mechanical energy sources.

Keywords: energy harvesting, responsive polymers, dielectric elastomers, passive energy harvesting, hydrogels

1. Introduction

Many modern applications, in which human intervention is either impossible or requires significant amount of human labor and time, demands a reliable, durable, and constant supply of energy. Examples of such applications include remote sensing, control-based applications, and IOT [1, 2]. Energy harvesting devices are one of the commonly employed solutions to this problem. Typically, these self-powered systems comprise three parts: (1) a transducer/harvester, which converts ambient power into usable electrical energy, (2) a battery to store the harvested energy, and (3) the final user, which utilizes the energy [3]. The transducer can be based on different conversion methods such as electromechanical [4], electromagnetic [5], triboelectric [6], acoustoelectric [7], thermoelectric [8], photoelectric [9], and chemoelectric [10].

* Author to whom any correspondence should be addressed.

Among them, the electromechanical mechanism is of particular interest since it can harness the mechanical energy available in several environments, such as natural or artificial vibrations, fluid motion, etc.

Energy harvesting from mechanical inputs is a well-known technology that exploits mechanical to electrical conversion with various materials and technologies [11]. Commonly, piezoelectric materials are employed to perform this conversion. However, stimuli-responsive polymers represent an interesting alternative to traditional energy harvesting approaches. Dielectric elastomers (DEs), which can experience large deformations in response to electric excitation [12, 13], as well as gels, capable of huge volumetric deformations upon solvent absorption [14–16], are examples of such materials. Commonly, DEs have been used for energy storage and energy harvesting by harnessing energy conversion mechanisms [17–19]. However, in the literature no particular attention has been focused on the mechanical energy source necessary to deform the DE material. Often, mechanical energy coming from human motion [20, 21] or vibrations of the environment [22] have been considered as suitable sources to harvest energy by using dielectric materials. Coupling hydrogels with highly deformable DEs provides the opportunity to convert mechanical energy, generated as a result of environmental conditions, to electrical energy. Broadly, this process takes advantage of the geometric deformations of DEs and the consequent change in electric capacitance [23–28], resulting in small-scale structures with high energy-density. For example, in VHB-type materials the measured harvested energy-density is on the order of magnitude of $\sim$10 mJ cm^{-3} with an efficiency of $\sim$20% for planar actuation and harvesting modes [29–31]. The work of Jiang *et al* [32] reported to produce $\sim$130 mJ cm^{-3} with an efficiency of $\sim$25% with the same material under a cone configuration.

Extensive studies have been conducted to understand the key parameters that govern the response of DE-based energy harvesting devices [33–35]. In addition, works that investigate the influence of material parameters [36–39], instability, and dissipation behavior [40–43] in DEs (such as VHB 4910) on the electro-mechanical coupling and the maximum theoretical energy-density are available. From an energy harvesting viewpoint, DE-based generators have been designed under different deformation modes such as equi-biaxial [36, 44–47], uniaxial [48], and conical stretch [29, 49, 50].

In this work, we propose a design for tubular DE-based energy harvesting devices. In such structures, the energy harvesting cycle includes four stages: (1) mechanically-induced inflation (i.e. an increase in mechanical energy), (2) electrically-induced dilation (i.e. an increase in the electromechanical energy), (3) deflation, or the removal of the mechanical loading, resulting in a decrease in mechanical energy and an increase in electrical energy, and (4) energy harvesting.

In currently available works, the initial inflation (or the first step) is achieved using an energy source that performs mechanical work. In the case of tubular structures, inflation can be achieved through the application of an internal pressure. The drawback of this deformation-inducing method is the need for a constant supply of energy, which limits the efficiency of the device. To overcome this drawback, we propose to exploit highly deformable stimulus-responsive materials. Specifically, the initial inflation can be obtained by the use of passive components that deform in response to environmental stimuli. Examples of such materials include liquid crystal elastomer (LCE) that expands due to thermal excitation [51–54] or hydrogels which swell as a result of water uptake [55–58]. The use of responsive materials enables autonomous use of the energy harvesting system and increases its efficiency.

In this contribution, we compare between active and passive charging approaches in DE-based tubular energy harvesting devices and demonstrate the capabilities of the design. We focus our attention on gels as the passive components. The paper is structured as follows: first, the energy harvesting cycle is presented and illustrated. Next, the kinematics and the governing equations for DE tubes which are subjected to electromechanical loading are summarized. We follow by studying the energy that can be harvested from DE tubes through active and passive charging. Lastly, we discuss the findings from this work and the merit of the design.

2. Energy harvesting with DE tubes

The concept of energy harvesting in DE-based tubular structures is described in figure 1. As shown in the transition from point 1 to point 2, consider a DE tube that radially inflates in response to internal pressure. This pressure can be applied directly or, alternatively, a stimulus-responsive cylinder can be placed inside the tube and expand radially due to changes in environmental conditions.

As a result of the inflating pressure, the tube dilates and gains mechanical energy. Next, the tube is electrically charged with a voltage V_3 (see transition from point 2 to point 3). Owing to its dielectric properties, the DE tube experiences additional electrically-induced dilation. The magnitude of the charge on the inner and the outer surfaces of the tube is $Q = V_3 C_3$.

Once the internal pressure is removed, the tube deflates and its radius decreases (see transition from point 3 to point 4). Practically, in stimulus-responsive materials the removal of the load is obtained through a change in environmental conditions. During this process, the total charge Q on the inner and the outer surfaces of the tube remains constant and the reduction in radius leads to a decrease in the capacitance C_4. As a result, the voltage increases to the value $V_4 = (C_3/C_4)\,V_3 > V_3$ and energy can be harvested to complete the cycle (point 4 to point 1).

The overall electrical energy gained in this process can be written as

$$E_{el} = \frac{1}{2} V_3^2 C_3 \left(\frac{C_3}{C_4} - 1 \right). \tag{1}$$

It is also convenient to define the energy-density per unit referential volume V_0 (also termed the volumetric energy-density) of the undeformed DE tube as follows,

$$e = \frac{E_{el}}{V_0}. \tag{2}$$

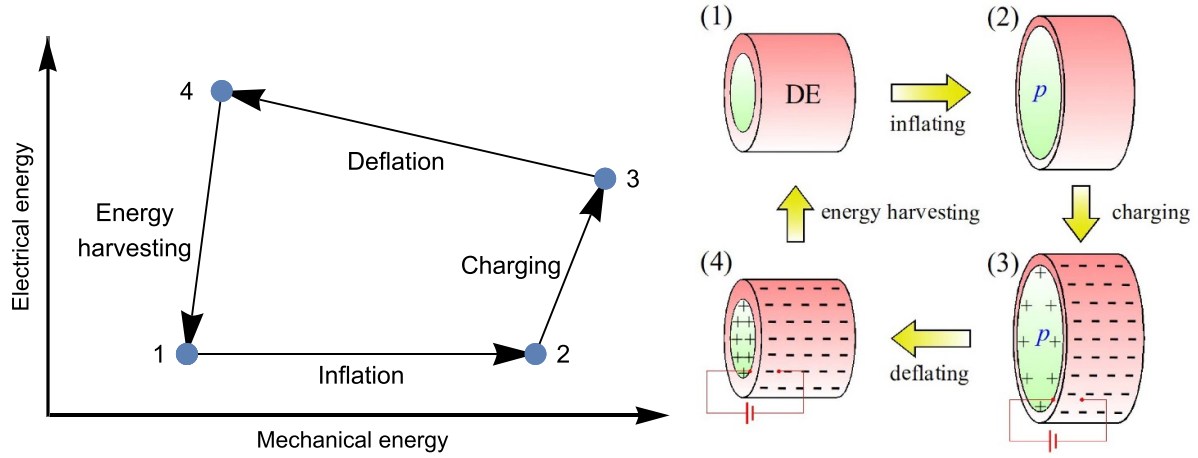

Figure 1. Energy harvesting cycle in DE tubes.

3. DE tubes—governing equations

Consider an infinite incompressible hyperelastic DE tube with a referential length L and inner and outer radii R_i and R_o, respectively. We introduce a polar coordinate system $\{R,\Theta,Z\}$ and denote the material points in the reference configuration via $R_i \leqslant R \leqslant R_o$, $0 \leqslant \Theta < 2\pi$, and $0 \leqslant Z \leqslant L$. The tube is subjected to an internal (inflation) pressure p and a potential difference $V = \Delta\phi$ along the radial direction. As a result, the tube dilates radially such that the inner and outer radii r_i and r_o, respectively, and the length l are achieved in the deformed configuration (see figure 2). The mapping of the material points can be written as

$$r = \sqrt{\frac{1}{\lambda}\left(R - R_i\right) + r_i};\ \theta = \Theta;\ z = \lambda Z, \tag{3}$$

and accordingly the deformation gradient is

$$\mathbf{F} = \begin{pmatrix} \frac{1}{\lambda}\frac{R}{r} & 0 & 0 \\ 0 & \frac{r}{R} & 0 \\ 0 & 0 & \lambda \end{pmatrix}. \tag{4}$$

Before proceeding, we recall the right Cauchy–Green strain tensor $\mathbf{C} = \mathbf{F}^T\mathbf{F}$ and note that due to the incompressibility assumed for the DE tubes, $J = \det\mathbf{F} = 1$.

From an electrical viewpoint, the electric field is determined from the electric potential via $\mathbf{E} = -\nabla\phi$, where the divergence operator is carried out with respect to the current (deformed) configuration of the system. The referential electric field is defined via $\mathbf{E}^{(0)} = \mathbf{F}^T\mathbf{E}$ [59].

The stress that develops in hyper-elastic DEs can be derived from a scalar strain energy-density function $\psi\left(\mathbf{F},\mathbf{E}^{(0)}\right)$. Following common practice, we assume that the strain energy-density function can be decomposed into two contributions,

$$\psi\left(\mathbf{F},\mathbf{E}^{(0)}\right) = \psi_m\left(\mathbf{F}\right) + \psi_c\left(\mathbf{F},\mathbf{E}^{(0)}\right), \tag{5}$$

where $\psi_m\left(\mathbf{F}\right)$ denotes the mechanical behavior in the absence of an electric field, and $\psi_c\left(\mathbf{F},\mathbf{E}^{(0)}\right)$ accounts for the coupled

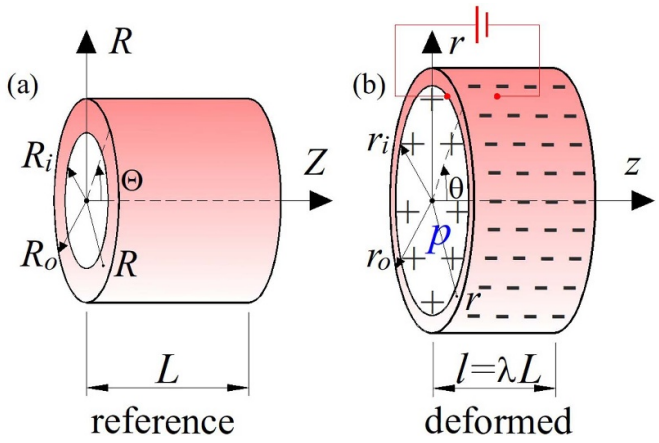

Figure 2. A schematic of the DE tube in the (a) reference and (b) inflated and charge states.

electro-mechanical response [59–61]. Accordingly, the stress tensor is

$$\boldsymbol{\sigma} = \frac{\partial\psi\left(\mathbf{F},\mathbf{E}^{(0)}\right)}{\partial\mathbf{F}}\mathbf{F}^T - \Pi\mathbf{I} = \boldsymbol{\sigma}_m + \boldsymbol{\sigma}_c - \Pi\mathbf{I}, \tag{6}$$

where $\boldsymbol{\sigma}_m = \partial\psi_m/\partial\mathbf{F}$ and $\boldsymbol{\sigma}_c = \partial\psi_c/\partial\mathbf{F}$ are the mechanical and the coupled electro-mechanical stress components, respectively, and $\Pi = \Pi(R)$ is a work-less pressure-like term that accounts for the incompressibility of the DE and is determined from the boundary conditions.

In this work, we consider isotropic DE tubes and consider a Yeoh-type energy-density function with n terms for the mechanical contribution,

$$\psi_m = \frac{1}{2}\left(\sum_{i=1}^{n}\frac{\alpha_i}{i}\left(I_1 - 3\right)^i\right), \tag{7}$$

where $I_1 = \mathrm{Tr}\left(\mathbf{C}\right)$ is the first invariant and α_i are material constants $(i = 1,\ldots,n)$. Note that in the case of $n = 1$, the neo-Hookean form $\psi_m = \frac{\alpha_1}{2}\left(I_1 - 3\right)$ is recovered. It can also be

shown that α_1 is the initial shear modulus of the DE. The inclusion of higher order α_i-terms can be used to account for the strain-induced stiffening effect, commonly observed in polymers.

As for the coupled electro-mechanical energy, we consider the form proposed by Dorfmann and Ogden [59],

$$\psi_c\left(\mathbf{F},\mathbf{E}^{(0)}\right) = -\frac{\varepsilon_r\varepsilon_0}{2}\mathbf{E}^{(0)}\cdot\mathbf{C}^{-1}\mathbf{E}^{(0)}, \tag{8}$$

where ε_r and ε_0 are the relative permittivity and the permittivity of vacuum, respectively.

The resulting Cauchy (true) stress tensor is computed by substituting equations (7) and (8) into equation (6),

$$\boldsymbol{\sigma} = \left(\sum_{i=1}^{n}\alpha_i\left(I_1-3\right)^{i-1}\right)\mathbf{F}\mathbf{F}^T + \varepsilon_r\varepsilon_0\mathbf{E}\otimes\mathbf{E} - \Pi\mathbf{I}. \tag{9}$$

From an electrical viewpoint, the applied potential difference V between the inner and the outer surfaces of the tube results in a radial electric field

$$\mathbf{E} = \frac{V}{\ln\left(r_o/r_i\right)}\frac{1}{r}\hat{\mathbf{r}}, \tag{10}$$

where $\hat{\mathbf{r}}$ is a unit vector along the radial direction. The capacitance is

$$C = \varepsilon_r\varepsilon_0\frac{2\pi l}{\ln\left(r_o/r_i\right)}, \tag{11}$$

and it is noted that the charge on the inner and outer surface is given by $Q = VC$.

To determine the equilibrium state, mechanical and electrical equilibrium as well as the boundary conditions must be satisfied. Due to the symmetry of the problem, the equilibrium equations along the θ and the z directions are automatically fulfilled. The only non-vanishing equation reads

$$\frac{\partial\sigma_{rr}}{\partial r} + \frac{\sigma_{rr}-\sigma_{\theta\theta}}{r} = 0, \tag{12}$$

where σ_{rr} and $\sigma_{\theta\theta}$ are the radial and the tangential stress components. The boundary conditions are given in terms of the radial and the longitudinal stress components. The tube is assumed to be traction free along its axis such that $2\pi\int_{r_i}^{r_o}\sigma_{zz}r\mathrm{d}r = 0$. Along the radial direction, the stress at the inner and the outer radii is prescribed (i.e. $\sigma_{rr}\left(R=R_i\right) = -p$ and $\sigma_{rr}\left(R=R_o\right) = 0$, where p is the inflation pressure).

To solve the boundary value problem, we solve the equilibrium equation (equation (12)) to determine the work-less pressure-like term $\Pi(R)$. Next, we employ the three boundary conditions and the incompressibility constraint to determine the deformed radii r_i and r_o and the deformed length l. Accordingly, we can determine the configuration of the tube in the mechanically inflated state, the charged state, and the deflated state.

Table 1. Geometry and material parameters used in the simulation.

Parameter	Notation and value
Inner radius of DE tube	$R_i = 1\,\mathrm{mm}$
Outer radius of DE tube	$R_o = 1.1\,\mathrm{mm}$
Permittivity of VHB 4910	$\varepsilon_r = 4.7$
Stiffness of VHB 4910	$\alpha_1 = G = 73\,\mathrm{kPa}$
Yeoh parameters for VHB 4910	$\alpha_2 = \alpha_3 = 0$, $\alpha_4 = G\cdot 10^{-3}\,\mathrm{kPa}$

4. Energy harvesting in DE tubes

In the following, we investigate the energy that can be harvested from a DE tube. To this end, we consider a tube with $R_i = 1\,\mathrm{mm}$, $R_o = 1.1\,\mathrm{mm}$, and $L = 10\,\mathrm{mm}$. The properties are taken as those of VHB 4910, which is an acrylic adhesive commonly employed as a DE [24, 32, 61–67]. Accordingly, we set the relative permittivity $\varepsilon_r = 4.7$ and the initial shear modulus $\alpha_1 = G = 73\,\mathrm{kPa}$. To show the influence of strain stiffening, we examine the neo-Hookean model and a Yeoh model with $\alpha_2 = \alpha_3 = 0$ and $\alpha_4 = G\cdot 10^{-3}\,\mathrm{kPa}$. All of the parameters are summarized in table 1. In addition, we define the dimensionless voltage $\tilde{V} = V/\left(R_o - R_i\right)\sqrt{\varepsilon_r\varepsilon_0/G}$.

4.1. Electro-mechanical response of a DE tube

Based on the theoretical framework illustrated above, figure 3(a) plots the normalized external pressure p/G in the absence of voltage ($\tilde{V} = 0$) as a function of the radial stretch r_i/R_i. As expected, the neo-Hookean model predicts a softening of the DE tube with increasing the pressure while the Yeoh model accounts for the experimentally observed stiffening and lock-up effect.

The normalized voltage $\tilde{V}$ as a function of the radial stretch r_i/R_i in the absence of pressure ($p/G = 0$) is depicted in figure 3(b). Note that the neo-Hookean model provides a response which reaches a peak voltage at $\tilde{V}\approx 0.7$, beyond which no solutions can be found. This non-physical behavior is a well-known drawback of the neo-Hookean model [61, 68]. The issue can be overcome by accounting for the strain-induced stiffening with the Yeoh model. This model predicts a snap-through of the tube at a critical voltage, followed by additional deformation and strain-induced stiffening.

In order to understand the harvesting mechanisms demonstrated in the next sections, it is worth emphasizing that the deformed configuration depends on the loading direction. Upon an increase in voltage, the DE tube snaps through at $\tilde{V}\approx 0.7$ such that the radial stretch increases from $r_i/R_i \approx 1.3$ to $r_i/R_i \approx 3.1$. Increasing the voltage results in further radial stretch. However, unloading from voltages that are above the critical value results in a reverse snap through from $r_i/R_i \approx 2.3$ to $r_i/R_i \approx 1.1$ at $\tilde{V}\approx 0.5$, thereby accessing different deformation states.

4.2. Active charging: mechanical inflation pressure

The active energy harvesting cycle, based on the application of a mechanical pressure (as described in section 2), is shown

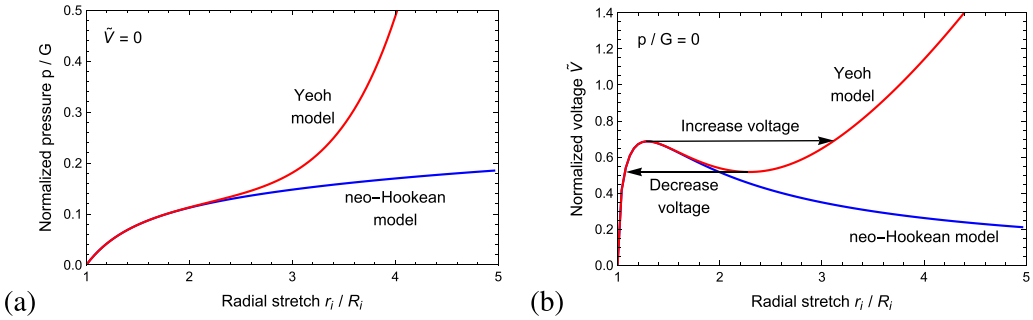

Figure 3. (a) Pressure p at $V = 0$ and (b) voltage V at $p = 0$ as a function of the inner radial stretch r_i/R_i.

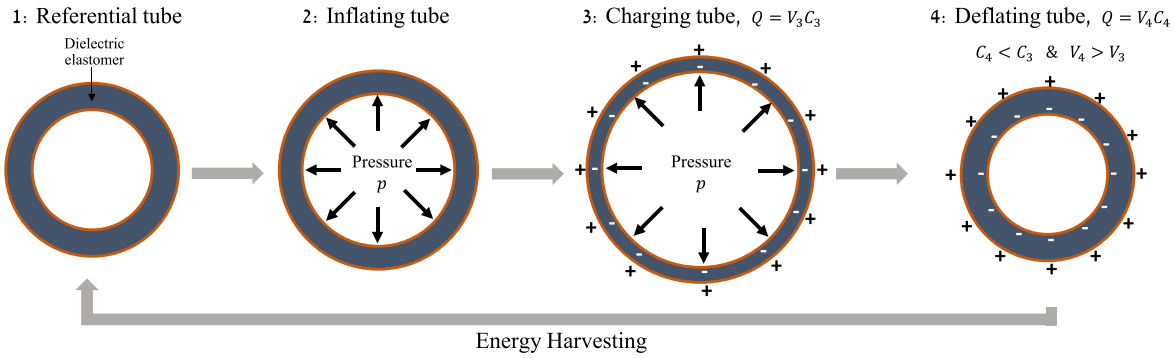

Figure 4. Energy harvesting in DE tubes: active charging using pressure.

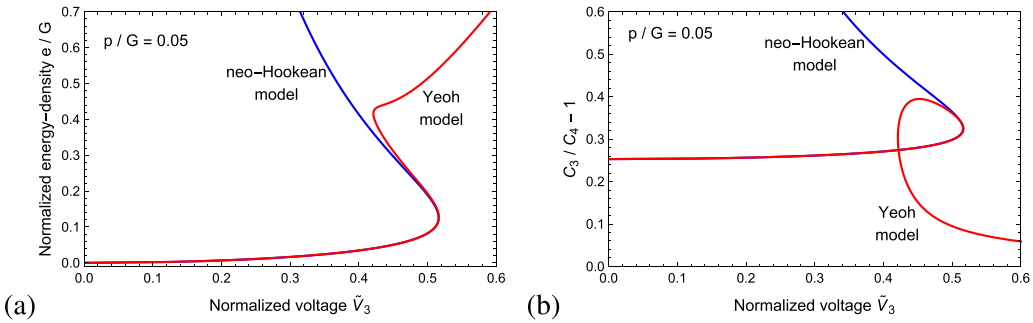

Figure 5. Normalized inflation pressure $p/G = 0.05$: (a) The normalized energy-density e/G and (b) the difference in the capacitance $C_3/C_4 - 1$ as a function of the normalized voltage $\tilde{V}_3$ for neo-Hookean and Yeoh materials.

in figure 4. First, the referential DE tube is shown. As a result of an applied inflation pressure p, the DE tube inflates (state 2). State 3 describes the configuration of the tube after it has been charged with a charge $Q = V_3C_3$, where V_3 and C_3 are the voltage and the capacitance in the charged loaded tube, respectively. Due to electrostatic forces, a further deformation takes place in the tube from state 2 to 3. Lastly, the inflation pressure is removed (i.e. the tube deflates) while the charge Q is maintained (see state 4). This leads to a decrease in the capacitance $C_4 < C_3$ and an increase in voltage $V_4 > V_3$.

In the following, we investigate the energy which can be harvested from the DE tubes. To this end, we define and set the normalized inflation pressure p/G and control the charging voltage $\tilde{V}_3$. It is emphasized that we assume that the material does not experience electrical breakdown, instabilities, or mechanical failure during the inflation and the charging process. In addition, it is worth noting that the inflation (which can be viewed as a prestretch of the material) allows for larger electrically induced deformations and thus reduces the likelihood of electrical breakdown [12, 69].

Figures 5(a) and (b) plot the normalized energy-density e/G and the difference in the capacitance $C_3/C_4 - 1$ as a function of the normalized voltage $\tilde{V}_3$, respectively, for the neo-Hookean and the Yeoh materials with an inflation pressure $p/G = 0.05$. In the inflation stage, the pressure is not sufficient to observe the strain-induced stiffening of the DE and accordingly the deformed configurations of the neo-Hookean and the Yeoh materials are similar. As expected, charging the DE tube with higher voltages $\tilde{V}_3$ leads to an increase in the harvested energy e.

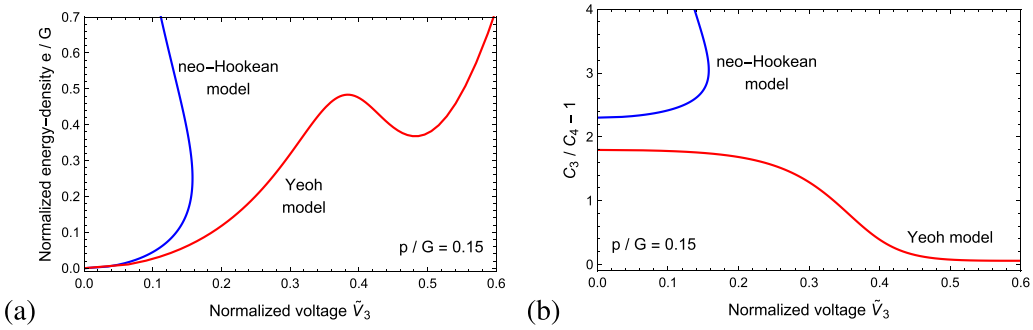

Figure 6. Normalized inflation pressure $p/G = 0.15$: (a) The normalized energy-density e/G and (b) the difference in the capacitance $C_3/C_4 - 1$ as a function of the normalized voltage $\tilde{V}_3$ for neo-Hookean and Yeoh materials.

The jump observed at $\tilde{V}_3 \approx 0.52$ is the result of the electrically induced snap through effect (illustrated in figure 3(b)). To understand the simulated trends, figure 5(b) plots the difference in the capacitance. We find that for neo-Hookean materials, once a peak voltage is reached, no other solutions can be found. However, in the Yeoh material, the quantity $C_3/C_4 - 1$ initially increases, reaches a peak value, and then loops back towards 0. The 'loop' stems from the electrically-induced snap through and the differences between the loading-unloading response shown in figure 3(b). The value of $C_3/C_4 - 1$ reaches zero at high voltages due to the stiffening effect, in which the difference between the conformations in stages 3 and 4 is small. However, we emphasize that the harvested energy depends on V_3^2, which is more dominant than the decrease in the capacitance ratio (see equation (1)).

The normalized energy-density e/G harvested for the higher normalized pressure $p/G = 0.15$ is shown in figure 6(a). While the neo-Hookean model exhibits roughly the same trend as under lower pressures, the Yeoh model predicts a different response. Specifically, we find that the harvested energy does not monotonically increases with voltage. This behavior is explained as follows: the inflation pressure deforms the DE tube and leads to strain-induced stiffening. If the applied voltage in state 3 is in the snap through region of a DE tube that is electrically excited without mechanical loading, then the removal of the inflation pressure results in conformations which can only be accessed along the unloading path shown in figure 3(b). This effect must be considered when designing an energy harvesting DE tube.

The difference in capacitance $C_3/C_4 - 1$ is shown in figure 6(b). As opposed to the case of $p/G = 0.05$, the quantity $C_3/C_4 - 1$ monotonically decreases with voltage according to the Yeoh model. This behavior stems from the application of a high inflation pressure, which deforms the tube into the strain-stiffening regime. This trend is also responsible for the drop $C_3/C_4 - 1 \to 0$ at high voltages, since the deformed configurations 3 and 4 are similar.

It is important to note that given the applied shear modulus G, the above-illustrated simulations predict a harvesting of energy-densities in the range of $\sim$10–50 mJ cm^{-3} with VHB 4910. This is comparable to available experimental findings for VHB-based generators [29–32]. Specifically, with $p/G = 0.15$ an electrical energy-density of $e \approx 15$ mJ cm^{-3} can be harvested at $V = 1$ kV. The work of Jiang *et al* [32] harvested $e \approx 12$ mJ cm^{-3} under an equivalent voltage in a cone DE generator with $Z = 60$ mm. At a voltage $V = 1.2$ kV, a circular ring generator, as proposed by Wang *et al* [17], is capable of harvesting $e \approx 11$ mJ cm^{-3}, while our design predicts $e \approx 20$ mJ cm^{-3}. We point out that the differences stem from the charging mode—in our design the DE is charged radially while in the work of Wang *et al* [17] the electric field acts across the film.

4.3. *Passive charging: swelling-induced inflation pressure*

The main disadvantage of the above-described DE-based energy harvesting device is the need for a constant input of active mechanical energy (in the form of work of inflation pressure). Here, we propose an alternative method to harvest energy using a passive charging mechanism. Specifically, as opposed to mechanically applying a pressure, materials that deform in response to a change in environmental conditions such as temperature, hydration, and presence of liquids, can be employed to passively charge the energy harvesting device. The advantage of this method is that an environmental source triggers the deformation and generates mechanical energy, which is stored in the DE tube. In the following, we consider polymeric gels as the passive component. The gels swell in the presence of an appropriate solvent due to gel-solvent affinity, and in turn exert inflation pressure on the DE tube. In the following we describe the concept illustrated in section 2 with respect to a passive charging mechanism.

To demonstrate this concept, consider a long cylindrical neo-Hookean dry polymeric gel that is placed in a DE tube. A thin insulating, impermeable, and highly deformable membrane is placed between the gel and the DE to prevent direct contact of the charges with the solvent permeating the gel (see state 1 in figure 7). Next, the inner part of the tube is filled with solvent and the gel swells. As a result, the gel applies a pressure that inflates the tube, thereby storing mechanical energy (see state 2 in figure 7). In state 3 of figure 7, the tube is charged with a charge $Q = V_3 C_3$. It is emphasized that in order to achieve a successful energy harvesting cycle, the contact between the gel, the insulating, impermeable, and

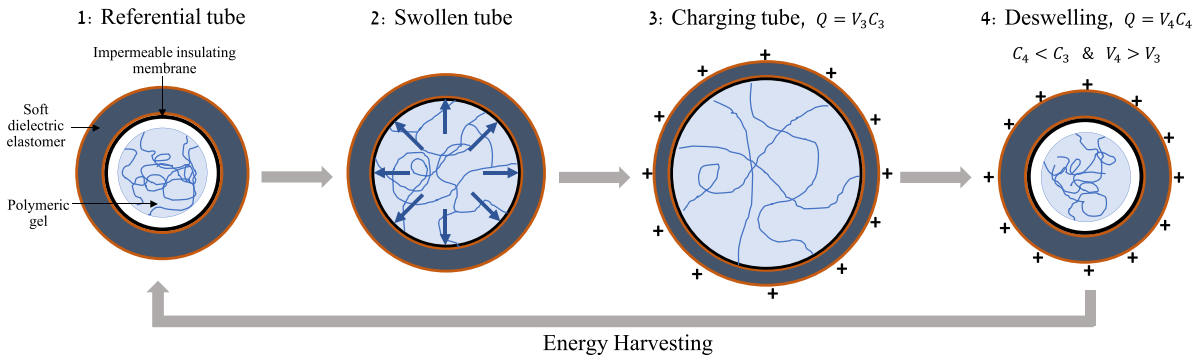

Figure 7. Energy harvesting in DE tubes: passive charging using swelling-induced forces.

highly deformable membrane, and the DE must be maintained. Practically, this leads to the requirement that the radial deformation of a freely swollen gel must be larger than the electrically induced radial stretch. Lastly, the solvent is drained out of the tube and the gel deswells (see state 4 in figure 7). As illustrated before for a mechanically applied inflation pressure, the charge is constant and therefore the capacitance $C_4 < C_3$ and the voltage $V_4 > V_3$. Consequently, electrical energy can be harvested from the DE tube. From a practical viewpoint, it is emphasized that deswelling is a slow process, and therefore this mechanism is useful as a battery rather than a fast power supply source.

In the following, we demonstrate the concept of passive charging. To this end, we summarize the governing equations and the boundary conditions of for the swelling of the constrained polymeric gels, as developed by Chester and Anand [70].

Consider a long cylindrical neo-Hookean dry polymeric gel with initial radius and length R_i and L_g, respectively. The material points are given in a polar coordinate system such that $0 \leqslant R \leqslant R_i$, $0 \leqslant \Theta < 2\pi$, and $0 \leqslant Z \leqslant L_g$. The gel is placed in a dielectric tube, which is coated with an insulating impermeable membrane. The inner part is then filled with water and the gel swells. As a result, the gel applies a pressure that leads to the dilation of the tube.

In the deformed configuration, the radius and length of the gel are r_i and l_g, respectively. The mapping of the material points is given by

$$r = \lambda_g R;\ \theta = \Theta;\ z = A_g Z, \tag{13}$$

where λ_g and A_g are the radial and the longitudinal stretches. Accordingly, the deformation gradient is

$$\mathbf{F}_g = \begin{pmatrix} \lambda_g & 0 & 0 \\ 0 & \lambda_g & 0 \\ 0 & 0 & A_g \end{pmatrix}, \tag{14}$$

where $J_g = \lambda_g^2 A_g$ is the volumetric deformation.

Following the framework of Chester and Anand [70], the stress that develops in the gel is

$$\boldsymbol{\sigma}_g = \frac{1}{J_g}\left(G_g \mathbf{F}_g \mathbf{F}_g^T - \Pi_g \mathbf{I}\right), \tag{15}$$

where G_g is the shear modulus of the dry gel and Π_g is a pressure-like term stemming from the solvent-polymer interactions and the mechanical interaction with the constraining tube. In addition, the chemical potential of the solvent molecules in the gel is given by

$$\mu = \mu^0 + kT\left(\ln\left(1 - \frac{1}{J_g}\right) + \frac{1}{J_g} + \chi\frac{1}{J_g^2}\right) + \frac{v}{J_g}\left(\Pi_g - G_g\right), \tag{16}$$

where k is the Boltzmann constant, T is the absolute temperature, μ^0 is a reference chemical potential, χ is the dimensionless interaction parameter governing the gel-solvent affinity.

The boundary conditions are employed to determine the swelling-induced pressure. Specifically, the gel is traction free along the longitudinal direction such that $\sigma_g^{(zz)} = 0$. Along the radial direction, the gel applies a radial stress that dilates the DE tube such that $\sigma_g^{(rr)}(R = R_i) = \sigma_{rr}(R = R_i)$. Lastly, chemical equilibrium requires that $\mu = \mu^0$.

To simulate the behavior of the system, we consider hydrogels and accordingly set the temperature and the volume of a water molecule $T = 300\,\mathrm{K}$ and $v = 3 \cdot 10^{-29}\,\mathrm{m}^3$, respectively. We begin by studying the configuration of the system in state 2, which results from the application of the passive gel component due to swelling. Figures 8(a) and (b) plot the stretch r_i/R_i of the gel tube as a function of the stiffness ratio G_g/G for selected values of χ in systems with neo-Hookean and Yeoh DE tubes, respectively. We find that extremely soft gels (i.e. $G_g/G \ll 1$) experience little swelling. This is due to the stiffness of the DE tube, which constrains the gels from dilating and expanding [71]. Stiffer gels with a shear modulus that is comparable to that of the DE exert larger swelling-induced stress on the tube and therefore experience significant radial swelling, resulting in higher mechanical energy of the DE tube. As can be seen, the radial stretch varies non-monotonically with the stiffness ratio, resulting in an optimum value G_g/G in both neo-Hookean and Yeoh tubes that leads to maximum radial stretch. This ratio is important since it governs the capacitance of the DE tube in state 3. In addition, note that lower interaction parameters, corresponding to gels with

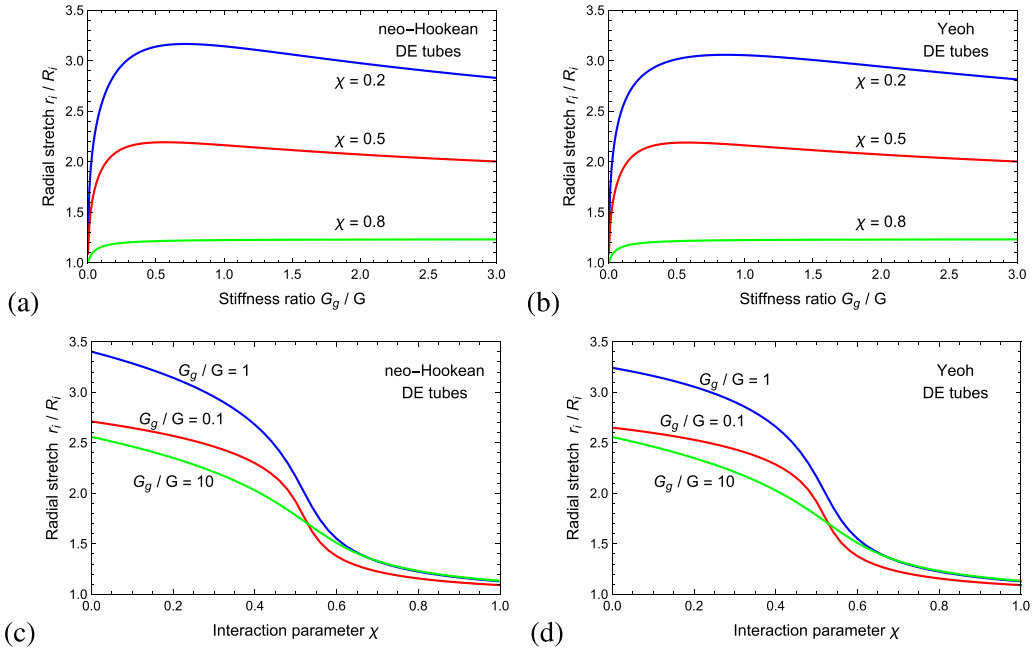

Figure 8. Passive mechanical loading using hydrogels: The radial stretch of the gel r_i/R_i as a function of (a), (b) the stiffness ratio G_g/G and (c), (d) the interaction parameter χ for neo-Hookean and Yeoh DE tubes.

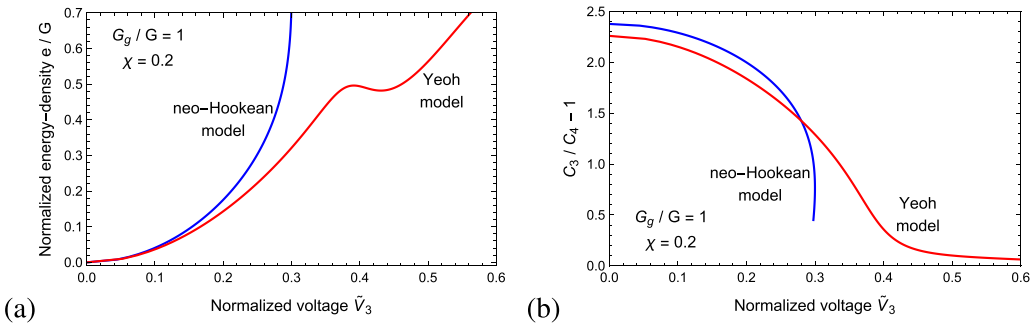

Figure 9. Energy harvesting using passive charging: (a) The normalized energy-density e/G and (b) the difference in the capacitance $C_3/C_4 - 1$ as a function of the normalized voltage $\tilde{V}_3$ for neo-Hookean and Yeoh materials.

a higher polymer-solvent affinity, result in increased swelling, as expected [16, 72, 73].

Figures 8(c) and (d) plot the stretch r_i/R_i of the gel tube as a function of the interaction parameter χ for three selected values of G_g/G in systems with neo-Hookean and Yeoh DE tubes, respectively. The interaction parameter governs the gel-solvent affinity, and therefore lower χ values result in a larger degree of swelling. The degree of swelling decays as the interaction parameter χ increases. These plots highlight the non-monotonous trends of the degree of swelling with the ratio G_g/G. Specifically, gels with a stiffness that is comparable to that of the DE tube experience significant swelling and apply interfacial pressures which are sufficient to significantly deform the tubes. In the case of $G_g/G = 0.1$, the gels cannot exert sufficient interfacial pressure to stretch the DE tube. Therefore, the behavior is governed by the gel-fluid affinity—lower values of χ lead to larger solvent uptake and radial stretch. Stiff gels, as shown via $G_g/G = 10$, are characterized by a high chain-density which mechanically hinders swelling. Therefore, the radial stretch obtained from such gels is smaller than with $G_g/G = 1$.

To investigate the energy harvesting capabilities of the gel-DE system, we choose the shear moduli ratio $G_g/G = 1$ and the dimensionless gel-fluid interaction parameter $\chi = 0.2$, a value that corresponds to a high gel-fluid affinity. Figures 9(a) and (b) plot the normalized energy-density e/G and the difference in the capacitance $C_3/C_4 - 1$ as a function of the normalized voltage $\tilde{V}_3$ for neo-Hookean and Yeoh materials. The observed trends suggest that the inflation pressure applied by the gel, resulting in state 2, deforms the tube to the stiffening regime, as explained in relation to the above discussed case characterized by $p/G = 0.15$ in the active charging (see figures 6(a) and (b). In addition, the electrical energy-density that can be harvested using passive charging is comparable to that obtainable with active charging under the examined properties. Specifically, under the voltages $V = 1\,\mathrm{kV}$and $V = 1.2\,\mathrm{kV}$, the energy-densities $e \approx 14\,\mathrm{mJ\,cm^{-3}}$ and $e \approx 18\,\mathrm{mJ\,cm^{-3}}$ can be harvested. This is comparable to

available experimental results. However, it is again emphasized that due to the diffusion mechanism that governs swelling, the charging is a slow process.

5. Conclusions

In this work, we explore the energy which can be harvested from DE tubes. To this end, we employ the neo-Hookean and the Yeoh models for the mechanical response of the DEs along with a well-known energy-density function that accounts for the electro-mechanical coupling. We begin by demonstrating the purely mechanical and the electro-mechanical response of DE tubes. As expected, the Yeoh model, which captures the strain-stiffening of elastomers, leads to the snap-through behavior under electric excitation.

Next, we investigate energy harvesting in two contexts: active charging and passive charging. In the former, the tube is inflated though an applied internal pressure. In the latter, a gel rod is placed in the tube and allowed to swell, resulting in inflation of the DE tube. Next, a voltage is applied across the tube, resulting in electro-mechanically induced deformations. Once the internal pressure or the gel are removed, energy can be harvested. Our simulations show that the energy-density which can be gained through an inflation-deflation cycle under active or passive charging is $\sim$10–50 mJ cm^{-3}, which is the same order of magnitude obtained in previous works with VHB DEs.

It is important to note that from a practical viewpoint, active charging can be used to quickly charge and harvest electrical energy from the device. The resulting electrical power is proportional to the rate of pressure increase/decrease. Accordingly, this design is useful in systems that require high electric power. Passive charging through gels is slow and governed by the diffusion of solvent molecules into the network. While this may be a drawback, the advantage of such a system is that no mechanical energy is required in order to charge (the radial deformation of the DE tube is through the autonomous swelling of the gel). This type of design can be used as an efficient energy source (or battery).

In conclusion, this work investigates energy harvesting in DE tubes and proposes a method to mechanically charge the system through unconventional environmental conditions using stimulus-responsive polymers. These systems can be used as a battery source that can be charged through ambient conditions, thereby providing a different approach for energy storage and supply in remote systems.

Data availability statement

All data that support the findings of this study are included within the article.

ORCID iDs

Roberto Brighenti https://orcid.org/0000-0002-9273-0822
Noy Cohen https://orcid.org/0000-0003-2224-640X

References

[1] Vo D T, Nguyen X P, Nguyen T D, Hidayat R, Huynh T T and Nguyen D T 2021 A review on the internet of thing (IoT) technologies in controlling ocean environment *Energy Sources*, *Part A: Recovery, Utilization, and Environmental Effects* 1–19
[2] Li W, Awais M, Ru W, Shi W, Ajmal M, Uddin S and Liu C 2020 Review of sensor network-based irrigation systems using IoT and remote sensing *Adv. Meteorol.* **2020** 1–14
[3] Akinaga H 2020 Recent advances and future prospects in energy harvesting technologies *Jpn. J. Appl. Phys.* **59** 110201
[4] Sezer N and Koc M 2021 A comprehensive review on the state-of-the-art of piezoelectric energy harvesting *Nano Energy* **80** 105567
[5] Carneiro P, Soares Dos Santos M, Rodrigues A, Ferreira J A F, Simoes J, Marques A and Kholkin A 2020 Electromagnetic energy harvesting using magnetic levitation architectures: a review *Appl. Energy* **260** 114191
[6] Lee B-Y, Kim D H, Park J, Park K-I, Lee K J and Jeong C K 2019 Modulation of surface physics and chemistry in triboelectric energy harvesting technologies *Sci. Technol. Adv. Mater.* **20** 758–73
[7] Lang C, Fang J, Shao H, Wang H, Yan G, Ding X and Lin T 2017 High-output acoustoelectric power generators from poly(vinylidenefluoride-co-trifluoroethylene) electrospun nano-nonwovens *Nano Energy* **35** 146–53
[8] Jaziri N, Boughamoura A, Müller J, Mezghani B, Tounsi F and Ismail M 2020 A comprehensive review of thermoelectric generators: technologies and common applications *Energy Rep.* **6** 264–87
[9] Sorokin A A, Bobashev S V, Feigl T, Tiedtke K, Wabnitz H and Richter M 2007 Photoelectric effect at ultrahigh intensities *Phys. Rev. Lett.* **99** 213002
[10] Xiao M, Wang L, Ji F and Shi F 2016 Converting chemical energy to electricity through a three-jaw mini-generator driven by the decomposition of hydrogen peroxide *ACS Appl. Mater. Interfaces* **8** 11403–11
[11] Zhou M, Al-Furjan M, Zou J and Liu W 2018 A review on heat and mechanical energy harvesting from human—principles, prototypes and perspectives *Renew. Sustain. Energy Rev.* **82** 3582–609
[12] Pelrine R, Kornbluh R, Pei Q and Joseph J 2000 High-speed electrically actuated elastomers with strain greater than 100% *Science* **287** 836–9
[13] Toupin R A 1956 The elastic dielectric *J. Ration. Mech. Anal.* **5** 849–915
[14] Brighenti R and Cosma M P 2022 Mechanics of multi-stimuli temperature-responsive hydrogels *J. Mech. Phys. Solids* **169** 105045
[15] Brighenti R, Cosma M P and Cohen N 2023 Mechanics and physics of the light-driven response of hydrogels *Mech. Res. Commun.* **129** 104077
[16] Cohen N 2019 Programming the equilibrium swelling response of heterogeneous polymeric gels *Int. J. Solids Struct.* **178-179** 81–90
[17] Wang Y, Zhu L, Zhang G, Zhong L and Chen H 2018 Capacitive energy harvesting using soft dielectric elastomers: design, testing and impedance matching optimization *AIP Adv.* **8** 085310
[18] Ren K, Liu Y, Hofmann H, Zhang Q M and Blottman J 2007 An active energy harvesting scheme with an electroactive polymer *Appl. Phys. Lett.* **91** 132910
[19] OHalloran A, OMalley F and McHugh P 2008 A review on dielectric elastomer actuators, technology, applications and challenges *J. Appl. Phys.* **104** 071101

[20] Riemer R and Shapiro A 2011 Biomechanical energy harvesting from human motion: theory, state of the art, design guidelines and future directions *J. NeuroEng. Rehabil.* **8** 22

[21] Gao S *et al* 2019 Wearable high-dielectric-constant polymers with core-shell liquid metal inclusions for biomechanical energy harvesting and a self-powered user interface *J. Mater. Chem.* A **7** 7109–17

[22] Yuan X, Changgeng S, Yan G and Zhenghong Z 2016 Application review of dielectric electroactive polymers (DEAPs) and piezoelectric materials for vibration energy harvesting *J. Phys.: Conf. Ser.* **744** 012077

[23] Pelrine R, Kornbluh R, Eckerle J, Jeuck P, Oh S, Pei Q and Stanford S 2001 Dielectric elastomers: generator mode fundamentals and applications *Proc. SPIE* **4329** 148–56

[24] Thomson G, Yurchenko D and Val D V 2018 *Energy Harvesting* (InTech)

[25] Hoffstadt T, Graf C and Maas J 2013 Optimization of the energy harvesting control for dielectric elastomer generators *Smart Mater. Struct.* **22** 094028

[26] Bortot E and Gei M 2015 Harvesting energy with load-driven dielectric elastomer annular membranes deforming out-of-plane *Extreme Mech. Lett.* **5** 62–73

[27] Bortot E, Gei M and deBotton G 2015 Optimal energy harvesting cycles for load-driven dielectric elastomer generators under equibiaxial deformation *Meccanica* **50** 2751–66

[28] Bortot E and Gei M 2015 Harvesting energy with an out-of-plane dielectric elastomer generator *Proc. Appl. Math. Mech.* **15** 379–80

[29] Wang H, Wang C and Yuan T 2012 On the energy conversion and efficiency of a dielectric electroactive polymer generator *Appl. Phys. Lett.* **101** 33904

[30] Wang H, Zhu Y, Wang L and Zhao J 2012 Experimental investigation on energy conversion for dielectric electroactive polymer generator *J. Intell. Mater. Syst. Struct.* **23** 885–95

[31] Jiang L, Betts A, Kennedy D and Jerrams S 2015 Investigation into the electromechanical properties of dielectric elastomers subjected to pre-stressing *Mater. Sci. Eng.* C **49** 754–60

[32] Jiang Y, Liu S, Zhong M, Zhang L, Ning N and Tian M 2020 Optimizing energy harvesting performance of cone dielectric elastomer generator based on VHB elastomer *Nano Energy* **71** 104606

[33] Kovacs G, During L, Michel S and Terrasi G 2009 Stacked dielectric elastomer actuator for tensile force transmission *Sens. Actuators* A **155** 299–307

[34] Mohd Ghazali F A, Mah C K, AbuZaiter A, Chee P S and Mohamed Ali M S 2017 Soft dielectric elastomer actuator micropump *Sens. Actuators* A **263** 276–84

[35] Mckay T, Rosset S, Anderson I and Shea H 2013 An electroactive polymer energy harvester for wireless sensor networks *J. Phys.: Conf. Ser.* **476** 2117

[36] Koh S, Keplinger C, Li T, Bauer S and Suo Z 2011 Dielectric elastomer generators: how much energy can be converted? *IEEE/ASME Trans. Mechatronics* **16** 33–41

[37] Chiang Foo C, Jin Adrian Koh S, Keplinger C, Kaltseis R, Bauer S and Suo Z 2012 Performance of dissipative dielectric elastomer generators *J. Appl. Phys.* **111** 094107

[38] Wu W, Jiang Y, Zhong M, Liu S, Yu B, Ning N, Tian M and Zhang L 2022 How do electromechanical properties of dielectric elastomer composites influence their energy harvesting performances? *Compos. Sci. Technol.* **228** 109639

[39] Cohen N, Oren S S and deBotton G 2017 The evolution of the dielectric constant in various polymers subjected to uniaxial stretch *Extreme Mech. Lett.* **16** 1–5

[40] Hong W 2011 Modeling viscoelastic dielectrics *J. Mech. Phys. Solids* **59** 637–50

[41] Chiang Foo C, Cai S, Jin Adrian Koh S, Bauer S and Suo Z 2012 Model of dissipative dielectric elastomers *J. Appl. Phys.* **111** 034102

[42] Li T, Qu S and Yang W 2012 Energy harvesting of dielectric elastomer generators concerning inhomogeneous fields and viscoelastic deformation *J. Appl. Phys.* **112** 034119

[43] Brighenti R, Menzel A and Vernerey F J 2018 A physics-based micromechanical model for electroactive viscoelastic polymers *J. Intell. Mater. Syst. Struct.* **29** 2902–18

[44] Lv X, Liu L, Liu Y and Leng J-S 2015 Dielectric elastomer energy harvesting: maximal converted energy, viscoelastic dissipation and a wave power generator *Smart Mater. Struct.* **24** 115036

[45] Zhao X and Suo Z 2009 Electromechanical instability in semicrystalline polymers *Appl. Phys. Lett.* **95** 031904

[46] Huang J, Shian S, Suo Z and Clarke D 2013 Dielectric elastomer generator with equi-biaxial mechanical loading for energy harvesting *Proc. SPIE* **8687** 86870Q

[47] Huang J, Shian S, Suo Z and Clarke D 2013 Maximizing the energy density of dielectric elastomer generators using equi-biaxial loading *Adv. Funct. Mater.* **23** 5056–61

[48] Graf C, Hitzbleck J, Feller T, Clauberg K, Wagner J, Krause J and Maas J 2013 Optimized energy harvesting materials and generator design *Proc. SPIE* **8687** 86870N

[49] Lee R, Basuli U, Lyu M, Kim E and Nah C 2014 Fabrication and performance of a donut-shaped generator based on dielectric elastomer *J. Appl. Polym. Sci.* **131** 40076

[50] Kornbluh R D, Pelrine R, Prahlad H, Wong-Foy A, McCoy B, Kim S, Eckerle J and Low T 2012 *Electroactivity in Polymeric Materials* ed L Rasmussen (Springer US) pp 67–93

[51] Warner M and Terentjev E M 1996 Nematic elastomers—a new state of matter? *Prog. Polym. Sci.* **21** 853–91

[52] Kent T A, Ford M J, Markvicka E J and Majidi C 2020 Soft actuators using liquid crystal elastomers with encapsulated liquid metal joule heaters *Multifunct. Mater.* **3** 025003

[53] Brighenti R and Cosma M P 2023 Multiphysics modelling of light-actuated liquid crystal elastomers *Proc. R. Soc.* A **479** 20220417

[54] Brighenti R and Cosma M P 2022 Smart actuation of liquid crystal elastomer elements: cross-link density-controlled response *Smart Mater. Struct.* **31** 015012

[55] Peppas N A, Bures P, Leobandung W and Ichikawa H 2000 Hydrogels in pharmaceutical formulations *Eur. J. Pharm. Biopharm.* **50** 27–46

[56] Ahmed E M 2015 Hydrogel: preparation, characterization and applications: a review *J. Adv. Res.* **6** 105–21

[57] Brannon-Peppas L and Harland R S 2012 *Absorbent Polymer Technology* (Elsevier)

[58] Okumura D and Chester S A 2018 Ultimate swelling described by limiting chain extensibility of swollen elastomers *Int. J. Mech. Sci.* **144** 531–9

[59] Dorfmann A and Ogden R W 2005 Nonlinear electroelasticity *Acta Mech.* **174** 167–83

[60] McMeeking R M, Landis C M and Jimenez S M A 2007 A principle of virtual work for combined electrostatic and mechanical loading of materials *Int. J. Nonlinear Mech.* **42** 831–8

[61] Cohen N 2017 Stacked dielectric tubes with electromechanically controlled radii *Int. J. Solids Struct.* **108** 40–48

[62] Kofod G, Sommer-Larsen P, Kornbluh R and Pelrine R 2003 Actuation response of polyacrylate dielectric elastomers *J. Intell. Mater. Syst. Struct.* **14** 787–93

[63] Bozlar M, Punckt C, Korkut S, Zhu J, Foo C C, Suo Z and Aksay I A 2012 Dielectric elastomer actuators with elastomeric electrodes *Appl. Phys. Lett.* **101** 091907
[64] Bazaev K and Cohen N 2022 Electrically-induced twist in geometrically incompatible dielectric elastomer tubes *Int. J. Solids Struct.* **250** 111707
[65] Moretti G, Papini G, Righi M, Forehand D, Ingram D, Vertechy R and Fontana M 2018 Resonant wave energy harvester based on dielectric elastomer generator *Smart Mater. Struct.* **27** 035015
[66] Hossain M, Vu D K and Steinmann P 2012 Experimental study and numerical modelling of VHB 4910 polymer *Comput. Mater. Sci.* **59** 65–74
[67] Hossain M, Vu D K and Steinmann P 2015 A comprehensive characterization of the electro-mechanically coupled properties of VHB 4910 polymer *Arch. Appl. Mech.* **85** 523–37
[68] Emuna N and Cohen N 2020 Inflation-induced twist in geometrically incompatible isotropic tubes *J. Appl. Mech.* **88** 031005
[69] Zurlo G, Destrade M, DeTommasi D and Puglisi G 2017 Catastrophic thinning of dielectric elastomers *Phys. Rev. Lett.* **118** 078001
[70] Chester S A and Anand L 2010 A coupled theory of fluid permeation and large deformations for elastomeric materials *J. Mech. Phys. Solids* **58** 1879–906
[71] Levin M and Cohen N 2023 Swelling under constraints: exploiting 3D-printing to optimize the performance of gel-based devices *Adv. Mater. Technol.* **8** 2202136
[72] Flory P J and Rehner J 1943 Statistical mechanics of cross-linked polymer networks I. Rubberlike elasticity *J. Chem. Phys.* **11** 512–20
[73] Flory P J 1953 *Principles of Polymer Chemistry* (Cornell University Press)